

Superconductivity and Electronic Structure of Perovskite MgCNi_3

D.J. Singh and I.I. Mazin

Center for Computational Materials Science,
Naval Research Laboratory, Washington, DC 20375, U.S.A.
(November 3, 2018)

The electronic structure, stability, electron phonon coupling and superconductivity of the non-oxide perovskite MgCNi_3 are studied using density functional calculations. The band structure is dominated by a Ni d derived density of states peak just below the Fermi energy, which leads to a moderate Stoner enhancement, placing MgCNi_3 in the range where spin fluctuations may noticeably affect transport, specific heat and superconductivity, providing a mechanism for reconciling various measures of the coupling λ . Strong electron phonon interactions are found for the octahedral rotation mode and may exist for other bond angle bending modes. The Fermi surface contains nearly cancelling hole and electron sheets that give unusual behavior of transport quantities particularly the thermopower. The results are discussed in relation to the superconductivity of MgCNi_3 .

The discovery¹ of superconductivity in the non-oxide perovskite MgCNi_3 , with critical temperature $T_c \approx 8\text{K}$, raises the questions of how superconductivity appears in such a Ni rich phase and its relationship to other unusual superconducting phases, particularly the Ni, Pd and Pt borocarbides and boronitrides^{2,3} and PdH.^{4–8} These possibly related materials have relatively high values of T_c and high concentrations of magnetic or near magnetic group 8 elements but different underlying physics.

Typically, but not always, perovskites are distorted by the freezing in of unstable zone boundary rotational phonons to form structures like the $Pnma$, GdFeO_3 structure or off-centerings like those that produce ferroelectricity as in BaTiO_3 . This is due to the importance of ionic and central interactions in many perovskites; the stability of the ideal cubic structure depends on a balance between A -site cation–anion and the B -site cation–anion interactions. In the minority that are truly cubic, there are often soft anharmonic phonons of displacive character, as *e.g.* in KTaO_3 and/or rotational character (the combination common in Pb based perovskites).⁹

According to refinements,¹ MgCNi_3 is stoichiometric with only a very small, 4% carbon deficiency and occurs in the ideal cubic perovskite structure. The ambient temperature lattice parameter is 3.812\AA , which yields a C–Ni bond length of 1.906\AA . Considering that Mg is expected to occur as Mg^{2+} and so the CNi_3 subunit as negatively charged, this bond may be considered short. As such, strong Ni–C covalent interactions are expected. If so and if bonding or antibonding electronic states associated with this are present at the Fermi energy E_F , strong electron phonon coupling (EPC) may be expected. Theoretical studies of the electronic structure and phonons showed that in fact EPCs associated with relatively hard modes that modulate strong bonds involving Ni and first row elements play an important role in the superconductivity of the borocarbides and nitrides.^{10–12}

On the other hand, the perovskite topology and the fact that Mg likely acts as a simple cation that is electronically inactive near E_F suggests that perhaps low frequency anharmonic modes play an important role. In

particular, phonon modes, like that associated with the octahedral rotation, will modulate the C–Ni–C bond angles, which in this structure are expected to be important in the hopping associated with metallic conduction. The crystal structure may be conceptually viewed as expanded fcc Ni with 25% of the sites replaced by Mg and C interstitials in octahedral sites. The bands thus should be narrow and transition metal-like around E_F with a higher filling than in pure Ni. This suggests some analogy with the band structure of PdH^{5,8}, also an expanded group 8 metal with a higher filling. The main difference is the important role of C as hopping mediator in MgCNi_3 , as discussed below.

The present experimental situation is confusing. Tunneling and upper critical field measurements were reported by Mao *et al.*¹³ These characterize MgCNi_3 as a strong coupling superconductor with an unusually large reduced energy gap, $2\Delta(0)/kT_c \approx 10$, near the upper theoretical limit¹⁴ for s -wave superconductivity. However, the specific heat jump $\Delta C(T_c)/kT_c \approx 1.9$ suggests moderate $\lambda \lesssim 1$ coupling.¹⁴ Furthermore, they suggested that MgNiC_3 may be a non- s superconductor, based on observation of a zero-bias anomaly (often, but not always, due to a sign-changing order parameter). This implies an analogy with metallic Pd where superconductivity is not observed, but a possible spin fluctuation mediated mechanism was discussed, or Sr_2RuO_4 , which is apparently a triplet superconductor due to spin fluctuations.¹⁵ On the other hand, doping with Co, a likely magnetic impurity, rapidly decreases the superconducting volume,^{16,17} and the same effect, but stronger, is found with Mn.¹⁷ Cu doping, however, reduces T_c without suppressing the superconducting fraction.¹⁶ This is consistent with expectations for s -wave pairing in a rigid band model. Hayward *et al.*¹⁶ reported a calculated electronic density of states (DOS) that shows a large peak just below E_F and speculated about the importance of magnetic fluctuations based on this.¹⁶ In this regard, doping on the Mg A -site may be illuminating as rigid band behavior may be more likely in that case.

Here we report electronic structure calculations focus-

ing on these issues. These were done in the local density approximation (LDA)¹⁸ with the general potential linearized augmented planewave (LAPW) method.¹⁹ Well converged zone samplings and basis sets, including local orbitals²⁰ to treat the Mg semicore states and relax linearization errors for the Ni d bands were used. The experimental lattice constant of $a=3.82\text{\AA}$ was used (our calculated LDA lattice parameter is 1.7% smaller as is typical for this approximation). We study the band structure and Fermiology, the susceptibility and proximity to magnetism, transport coefficients and selected phonon modes and electron-phonon couplings. Transport coefficients were determined using kinetic theory²¹ with zone integrations using LAPW eigenvalues on a grid of 2925 \mathbf{k} -points in the irreducible $1/48$ wedge.

The band structure and DOS are shown in Figs. 1 and 2. The Fermi surfaces are in Fig. 3. As expected, Mg plays an minor role in the bands in the valence region. (There is a weak Ni d -Mg s bonding interaction. The Γ point state at -6 eV has Mg-Ni bonding character with the corresponding antibonding state at +3 eV. This covalency is localized around Γ). Octahedral coordination is unfavorable for formation of C sp hybrids, so not surprisingly the C s orbitals are also inactive. They occur around -12 eV (relative to E_F) and are not shown. The valence region, which extends from -7.1 eV to +1 eV is therefore derived from the 15 Ni d and 3 C p orbitals filled by 34 electrons. The C p orbitals are strongly hybridized with Ni d , and are located below most of the d states. So in the first approximation they can be integrated out and the bands near the Fermi level can be analyzed in terms of the Ni d states.

The unusual two-fold linear Ni coordination by C makes some of the bands very narrow. For instance, Ni(x) yz and $y^2 - z^2$, Ni(y) zx and $z^2 - x^2$, and Ni(x) xy and $x^2 - y^2$ orbitals do not disperse in the nearest neighbor approximation (NNA) as they have no C orbitals to hop through.²² The remaining 9 orbitals form three independent manifolds, consisting of Ni(x) xy , Ni(z) yz , and Ni(y) $y^2 - r^2$ orbitals, coupled via C p_y and the two corresponding combinations (*i.e.* p_x and p_z). Interestingly, in the NNA, one of the three resulting bands in each manifold, the one that involves the antibonding combination of the t_{2g} orbitals, is non-bonding again. The result is 3 bonding, 3 nonbonding and 3 antibonding bands. Two of these antibonding bands cross E_F . In the large crystal field limit (relative to the small widths), these have a simple dispersion proportional to $\sin(ak_x/2)^2 + \sin(ak_y/2)^2$ etc., which naturally makes them flat for a number of high-symmetry directions. This is reflected in the Fermi surface (Fig. 3). The lower band produces Γ centered rounded cube shaped electron sections and a narrow low weight jungle gym along the $R - M$ lines also containing electrons. The upper band (Fig. 3 bottom) forms a two-sheet Fermi surface consisting of pancaked squares centered at the X points and ovoids along the $\Gamma - R$ lines, both hole-like. The flat square shape reflects weak dispersion of the underlying band along $X - M$ and strong

dispersion along $X - \Gamma$ (The quasi-2D behavior is because $\sin(ak_x/2)^2 + \sin(ak_y/2)^2$ does not disperse along z .) Near Γ , where these bands make up the three fold degenerate state (this is the second one below E_F), the dispersion is due to direct Ni-Ni $dd\sigma$ hopping. Turning to the two bands that cross E_F , the lower band forms the more interesting heavy sheet of Fermi surface around X . At an M point, say (110), $\sin(ak_x/2)^2 + \sin(ak_z/2)^2$ and $\sin(ak_y/2)^2 + \sin(ak_z/2)^2$ are degenerate and their hybridization via Ni(x) xy and Ni(y) xy orbitals is proportional to $\cos(ak_x/2)\cos(ak_y/2)$ and vanishes near M , which is why they are heavy. On lowering E_F , the X centered squares grow grow, as does DOS at E_F , $N(E_F)$, until they meet at the M points and the topology changes.

The value of $N(E_F)$ is 4.99 eV^{-1} on a per formula unit basis. Two recent non-full-potential studies obtain differing values. Dugdale and Jarlborg report 6.35 eV^{-1} and 3.49 eV^{-1} depending on the exact method they employ,²³ while Shim and Min obtain 5.34 eV^{-1} , which is much closer to the present result.²⁴ These differences are significant as they control the proximity to magnetism. In particular, the susceptibility, $\chi(0)$, is determined by $N(E_F)/(1 - N(E_F)I)$, where I is the Stoner parameter, and the denominator contains a small difference involving $N(E_F)$. Comparing our calculated full potential $N(E_F)$ with the experimental linear coefficient $\gamma \approx 10 \text{ mJ/moleNiK}^2$, we obtain a specific heat renormalization $\gamma/\gamma_{band}=2.6$. The calculated plasma frequency is $\hbar\omega_P = 3.25 \text{ eV}$. The calculated Hall number is $-1.3 \times 10^{22} \text{ cm}^{-3}$. This agrees well with the measured value of Li *et al.*²⁵ The constant scattering time approximation thermopower, S , is p -type except at very low T below 10K where it is n -type consistent with the Hall number. S is very small (less than $1 \mu\text{V/K}$) below 150K but then rises more rapidly reaching $5 \mu\text{V/K}$ at 300K and $16 \mu\text{V/K}$ at 600K. Both the Hall number and the thermopower are controlled by the competition between the hole and electron pockets of comparable size, which leads, for instance, to the unusual T -dependence of thermopower. Using the calculated ω_P and the measured resistivity^{1,25} in the Bloch-Gruneisen formula, $d\rho/dT = (8\pi^2/\hbar\omega_P^2)k_B\lambda_{tr}$, we obtain $\lambda_{tr} \approx 1 - 1.6$, though we note that this extraction of λ_{tr} is sensitive to sample quality.

The simplest estimate of λ from zone center frozen-phonon calculations is not applicable to cubic perovskites since no zone-center modes couple by symmetry. However one can use frozen-phonon zone-corner calculations for this purpose, as in Ref. 26. The relevant formula is

$$\begin{aligned} \lambda &= \sum_{\nu\mathbf{q}} \lambda_{\nu\mathbf{q}} \approx \frac{2}{N_{\uparrow}\omega_{\nu\mathbf{q}}} \sum_{\nu} \langle |g^{\nu}|^2 \rangle \sum_{n,m,\mathbf{k},\mathbf{q}} \delta(\varepsilon_{n,\mathbf{k}+\mathbf{q}})\delta(\varepsilon_{m,\mathbf{k}}) \\ &= 2N_{\uparrow} \sum_{\nu} \langle |g^{\nu}|^2 / \omega_{\nu\mathbf{q}} \rangle \end{aligned}$$

Here N_{\uparrow} is the per spin DOS at E_F , and g^{ν} is an electron-ion matrix element from the derivative of the ionic potential with respect to the dimensionless phonon

coordinate (see Ref. 26 for details). To get qualitative information on the EPC, we focus on two R-point phonons. These are the octahedral rotation and the fully symmetric breathing mode. The former mode changes the C-Ni-C bond angles, but not the bond lengths in lowest order, while the latter is a pure bond stretching mode. The calculated frequencies are 105 cm^{-1} and 349 cm^{-1} , respectively.

To estimate the matrix element, we selected several points on the intersection line of the \mathbf{k} and $\mathbf{k}+\mathbf{q}$ Fermi surfaces, and fitted the bands in the nearby region with the second-order perturbation theory, and then averaged the resulting matrix element. We included three intersection points, where g does not vanish by symmetry, for the breathing mode, and 7 points for the rotational mode. Assuming that averaging over \mathbf{q} does not change g^2 , we find for the breathing mode $\lambda \approx 0.005$ and for the rotational mode $\lambda \approx 1.2$. The latter dominates not only because of its nearly 4 times larger deformation potential and its 15 times smaller denominator $M\omega^2$. Because of the mode degeneracy, this corresponds to a total rotational modes $\lambda_{rot} \approx 3.6$. However, in oxide perovskites, this R_{25} rotation mode usually stiffens rapidly away from the zone boundary, reflecting the rigidity of the O octahedra. Here such a stiffening may also be expected. Thus, the zone averaged λ will likely be considerable smaller, but probably still substantial. In any case, it can be said that the stiff C-Ni bond stretching modes are apparently not significant contributors to the EPC, while rotational (and probably other C-Ni-C bond bending) modes are strongly coupled. Note that the popular rigid muffin-tin potential method is hard to apply here: for transition metals, it is known to overestimate EPC, and Ni is in a low-symmetry position. Most importantly, with such a large disparity of the contributions from different modes, there is no telling beforehand, which average phonon frequency should be used in calculating λ .

As mentioned, possible nearness a magnetism could conceivably play an important role. To investigate this, we have calculated spin susceptibility directly from the variation of the total energy with small imposed magnetizations (ranging from 0.1 to $0.7\ \mu_B$ per cell) in fixed spin moment calculations, $\delta E_{tot} = \chi^{-1}m^2/2 = (N_{\uparrow}^{-1} - I)m^2/4$, where I is the Stoner factor, characterizing intraatomic exchange (for a compound like MgCNi_3 , I is expected to be close to 1/3 of the pure Ni value of 1.16 eV, probably slightly reduced because of hybridization with C). It appears that $\delta E_{tot}(m)$ noticeably deviates from the quadratic behavior. This is expected in extended Stoner theory,²⁷ where an average $\tilde{N}(m)$ is substituted for N_{\uparrow} . With $\tilde{N}(m)$, the above expression gives a good description of $\delta E_{tot}(m)$ up to $m \leq 0.6\ \mu_B$ with a weakly energy dependent $I \approx 0.95/3$ eV. Self-consistent virtual crystal calculations corresponding to a 10% replacement of Mg by a monovalent element (Na in the calculations but with the lattice parameter fixed - so Li or a 5% Mg deficiency may be a better experimental

analogue) produced a borderline ferromagnetic ground state with a very low energy gain and a moment of $0.25\ \mu_B/\text{cell}$.

The susceptibility renormalization $(1 - IN_{\uparrow})^{-1} \approx 5$, and $\chi = 2.7 \times 10^{-4}\text{ emu/moleNi}$, somewhat larger than the reported experimental value¹⁶ of $1.7/\text{times}10^{-4}\text{ emu/moleNi}$. This number is expected to be very sensitive to doping, *i.e.* composition, due to the near cancellation in the denominator. Perhaps the difference with experiment can be understood in these terms *e.g.* if the 4% of C vacancies lead to a higher effective band filling. If the Stoner renormalization is indeed ≈ 5 , this signals presence of significant spin fluctuations. To compare with, in Sr_2RuO_4 , where $(1 - IN_{\uparrow})^{-1} \approx 9$, spin fluctuations are believed to cause triplet superconductivity, and in Pd metal, where it is ≈ 30 , spin fluctuations destroy superconductivity which would otherwise exist due to the sizeable ($\lambda \gtrsim 0.5$) EPC. Importantly, the effect of spin fluctuations on mass renormalization, transport and superconducting properties is very different: essentially, in the first two cases, the coupling constants add, while for superconductivity they add in the mass renormalization term, and subtract in the pairing term (In the strong coupling T_c is not proportional to $\exp[-(1 + \lambda)/\lambda]$, but rather $\exp[-(1 + \lambda_{ph} + \lambda_{spin})/(\lambda_{ph} - \lambda_{spin})]$.) This may explain the inconsistency between coupling constants determined from different experiments.

In any case, the present results underscore certain similarities with PdH in terms of band structure and magnetic renormalizations, as well as with the borocarbides. However, the fact that the most important phonons are Ni bond-bending modes places MgCNi_3 in a unique class of its own.

This work is supported by ONR and the ASC computer center.

¹ T. He, *et al.*, Nature **411**, 54 (2001).

² R. Nagarajan, *et al.*, Phys. Rev. Lett. **72**, 274 (1994).

³ R.J. Cava, *et al.*, Nature **367**, 146 (1994); R.J. Cava, *et al.*, Nature **367**, 252 (1994). R.J. Cava, *et al.*, Phys. Rev. B **49**, 12384 (1994); R.J. Cava, *et al.*, Nature **372**, 245 (1994).

⁴ T. Skoskiewicz, Phys. Status Solidi A **11**, K123 (1972).

⁵ D.A. Papaconstantopoulos, B.M. Klein, J.S. Faulkner, and L.L. Boyer, Phys. Rev. B **18**, 2784 (1978).

⁶ J.M. Rowe, *et al.*, Phys. Rev. Lett. **33**, 1297 (1974).

⁷ A. Rahman, *et al.*, Phys. Rev. B **14**, 3630 (1976).

⁸ B.M. Klein, and R.E. Cohen, Phys. Rev. B **45**, 12405 (1992).

⁹ M. Fornari, and D.J. Singh, Phys. Rev. B **63**, 092101 (2001).

¹⁰ L.F. Mattheiss, T. Siegrist, and R.J. Cava, Solid State Commun. **91**, 587 (1994).

¹¹ W.E. Pickett, and D.J. Singh, Phys. Rev. Lett. **72**, 3702

- (1994).
- ¹² D.J. Singh, and W.E. Pickett, Phys. Rev. B **51**, 8668 (1995).
- ¹³ Z.Q. Mao, *et al.*, cond-mat/0105280.
- ¹⁴ J.P. Carbotte, Rev. Mod. Phys. **62**, 1027 (1990).
- ¹⁵ Y. Maeno, *et al.*, Nature **372**, 532 (1994).
- ¹⁶ M.A. Hayward, *et al.*, cond-mat/0104541.
- ¹⁷ Z.A. Ren, *et al.*, cond-mat/0105366.
- ¹⁸ L. Hedin, and B. I. Lundqvist, J. Phys. C **4**, 2064 (1971).
- ¹⁹ D.J. Singh, *Planewaves, Pseudopotentials and the LAPW Method* (Kluwer Academic, Boston, 1994).
- ²⁰ D. Singh, Phys. Rev. B **43**, 6388 (1991).
- ²¹ J.M. Ziman, Principles of the Theory of Solids (Cambridge University Press, Cambridge, 1972), and references therein.
- ²² Ni has tetragonal symmetry with the axis directed towards the two neighboring C. We use Ni(x) to denote the Ni with tetragonal axis along x.
- ²³ S.B. Dugdale, and T. Jarlborg, preprint (cond-mat/0105349).
- ²⁴ J.H. Shim, and B.I. Min, preprint (cond-mat/0105418).
- ²⁵ S.Y. Li, *et al.*, cond-mat/0104554.
- ²⁶ A.I. Lichtenstein, *et al.*, Phys. Rev. B **44**, 5388 (1991).
- ²⁷ G.L. Krasko, Phys. Rev. B **36**, 8565 (1987).

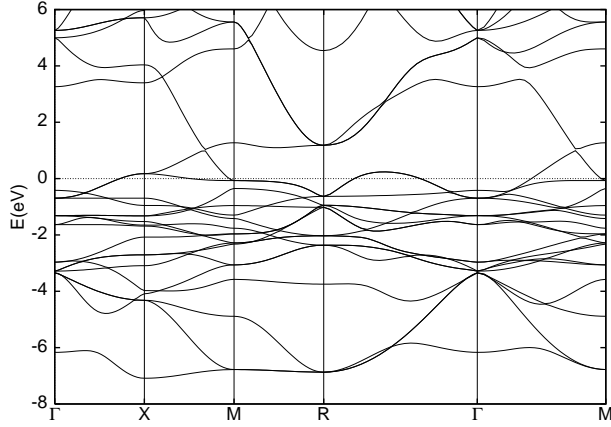


FIG. 1. LDA band structure of MgCNi₃. E_F is at 0.

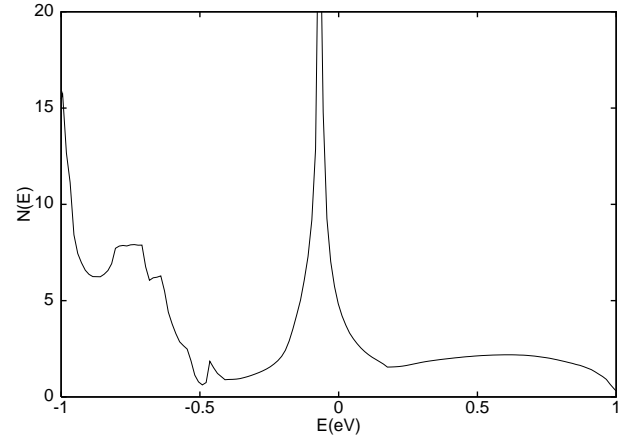
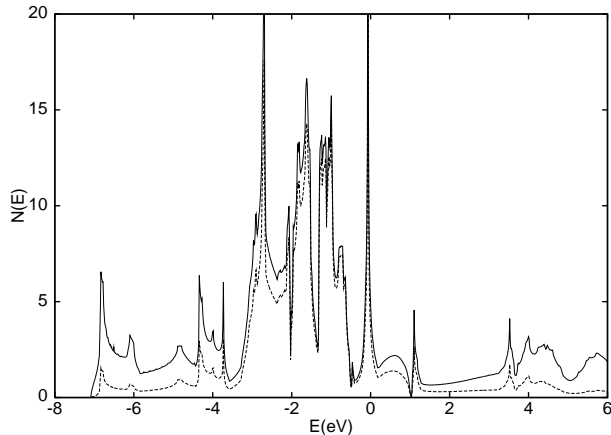
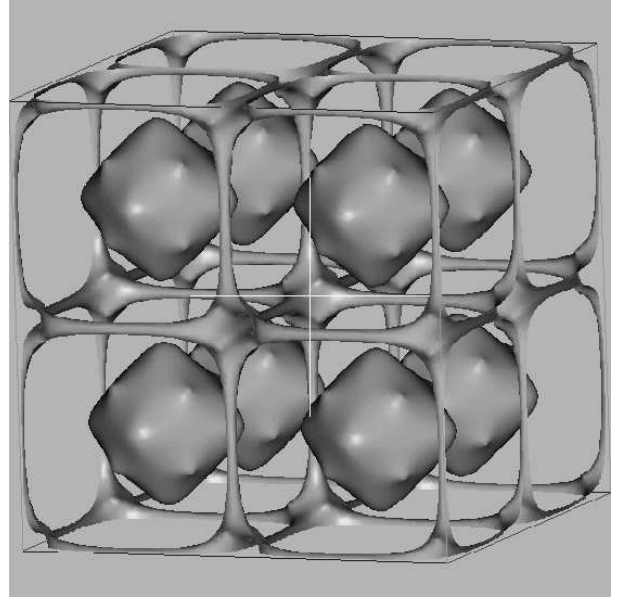


FIG. 2. Electronic DOS (upper panel) of MgCNi₃ as calculated within the LDA. The dashed line is the d contribution within the Ni LAPW spheres of radius $2.04 a_0$. The lower panel is a blow-up around E_F .



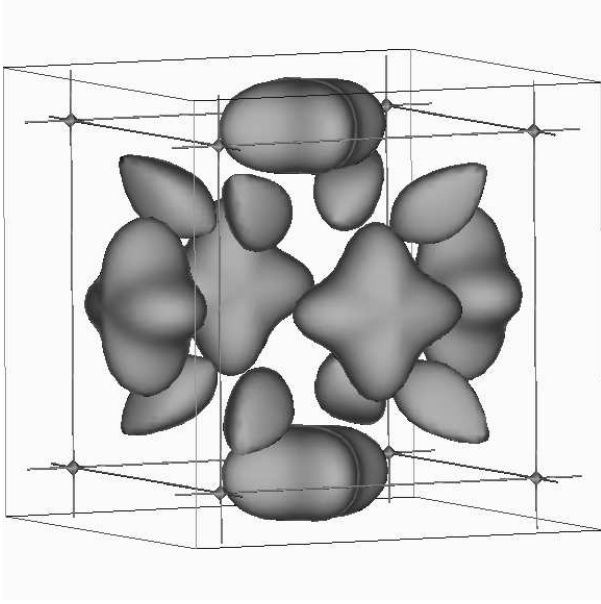


FIG. 3. Calculated Fermi surfaces. The top panel is from the lower band and shows eight zones. The rounded cube sections are centered at Γ , while the thin jungle gym is along the $M-R$ lines. The bottom panel is from the upper band, showing dimpled square shaped sections centered at X and ovoids along $\Gamma-R$.